

ARTICLE

Received 19 Jun 2015 | Accepted 15 Sep 2015 | Published 19 Oct 2015

DOI: 10.1038/ncomms9663

OPEN

High-performance mussel-inspired adhesives of reduced complexity

B. Kollbe Ahn^{1,*}, Saurabh Das^{2,*}, Roscoe Linstadt³, Yair Kaufman², Nadine R. Martinez-Rodriguez⁴, Razieh Mirshafian¹, Ellina Kesselman⁵, Yeshayahu Talmon⁵, Bruce H. Lipshutz³, Jacob N. Israelachvili² & J. Herbert Waite⁴

Despite the recent progress in and demand for wet adhesives, practical underwater adhesion remains limited or non-existent for diverse applications. Translation of mussel-inspired wet adhesion typically entails catechol functionalization of polymers and/or polyelectrolytes, and solution processing of many complex components and steps that require optimization and stabilization. Here we reduced the complexity of a wet adhesive primer to synthetic low-molecular-weight catecholic zwitterionic surfactants that show very strong adhesion ($\sim 50 \text{ mJ m}^{-2}$) and retain the ability to coacervate. This catecholic zwitterion adheres to diverse surfaces and self-assembles into a molecularly smooth, thin ($< 4 \text{ nm}$) and strong glue layer. The catecholic zwitterion holds particular promise as an adhesive for nanofabrication. This study significantly simplifies bio-inspired themes for wet adhesion by combining catechol with hydrophobic and electrostatic functional groups in a small molecule.

¹Marine Science Institute, University of California, Santa Barbara, California 93106, USA. ²Chemical Engineering, University of California, Santa Barbara, California 93106, USA. ³Chemistry and Biochemistry, University of California, Santa Barbara, California 93106, USA. ⁴Molecular, Cellular and Developmental Biology, University of California, Santa Barbara, California 93106, USA. ⁵Chemical Engineering, Technion-Israel Institute of Technology, Haifa 3200003, Israel. * These authors contributed equally to this work. Correspondence and requests for materials should be addressed to J.N.I. (email: jacob@engineering.ucsb.edu) or to J.H.W. (email: waite@lifesci.ucsb.edu).

Marine mussels attach to rocks by way of thread-like tethers on wind- and wave-swept seashores where wave velocities can reach 25 ms^{-1} . Mussel attachment tenacity is enabled by adaptations at multiple length scales¹, and the nanometre scale corresponds most closely to the chemistry of the interface². Interfacial mussel foot proteins (mfps), especially mfp-3 and mfp-5, are rich in the catecholic amino acid, 3,4-dihydroxyphenylalanine (Dopa), which has been adopted for functionalizing diverse synthetic polymers^{3,4}. Although the role of Dopa in wet adhesion is under increasing scrutiny, its introduction into polymers often endows them with strong underwater adhesion^{2,4,5} and self-healing^{6–8} capabilities. Other common amino acids, for example, lysine, phosphoserine and histidine, are also relevant to mfp adhesion^{9,10} and merit translation to synthetic systems^{4,11}. Mfps are protein polyelectrolytes with high charge densities¹², and lend themselves to complex coacervation, which appears to be critical for the lossless fluidic delivery of mfps to target surfaces underwater^{9,12}. Lysine and phosphoserine have been adopted to enhance adsorption¹¹, but also to drive charge-dependent complexation¹³ needed for the dense fluid phase separation (coacervation) of adhesive polyelectrolytes from the equilibrium solution. Of particular interest here, mfp-5 and -3 function as adhesive primers¹⁴ at the plaque–substratum interface¹⁵. Despite recent progress in the science of wet adhesion, practical underwater adhesion remains limited or non-existent for a variety of potential applications. Biomimetic synthetic initiatives have aspired to remedy this by mimicking specific attributes of the bioadhesive model systems of mussels and sandcastle worms. These attributes include macromolecular adsorption to surfaces^{2,3,16,17}, fluid–fluid phase separation (coacervation)^{13,18} and curing by oxidative catechol-based crosslinking^{2,19,20},

and involve many complex components and steps requiring optimization and stabilization²¹.

In this study, both the strong wet adhesion²² of mfp-5 films and the coacervation⁹ of mfp-3 were translated into a smaller and simpler zwitterionic platform. We sought to simplify and combine several motifs borrowed from the interfacial adhesive mfps (including catechol, positive and negative charges, and nonpolar moieties) into a single, low-molecular-weight, one-component adhesive system. By taking a previously reported gemini zwitterionic surfactant²³ with charged quaternary amine and phosphate groups and two alkyl tails, we replaced one of the tails with a catechol, and varied the other tail to create a family of mfp-mimetic zwitterionic adhesive homologues (mass < 500 Da). These homologues exhibit very strong and spontaneous catechol-mediated binding to surfaces, stable phase separation as one-component coacervates or bilayer films, and periodate-mediated curing. The measured adhesion energy ($W_{\text{ad}} \sim 50 \text{ mJ m}^{-2}$) is the highest reported to date^{22,24} for a nm-thick film formed underwater, and 2–3 times greater than mfp-5 (ref. 22) or the recently engineered recombinant mfp–amyloid fusion protein²⁴. Zwitterion-mediated adhesion is likely to stimulate applications at multiple length scales including nanofabrications^{25,26} that require molecularly smooth and thin (< 4 nm) adhesive layers, for example, in electronic²⁷, lithographic²⁸ and biomedical applications².

Results

Zwitterionic adhesives design inspiration. The phosphate, amine, catechol and hydrophobic (alkyl or benzyl) functionalities in the zwitterions were adopted from the following mole percents of amino-acid residues in mfp-5, for example, anionic residues

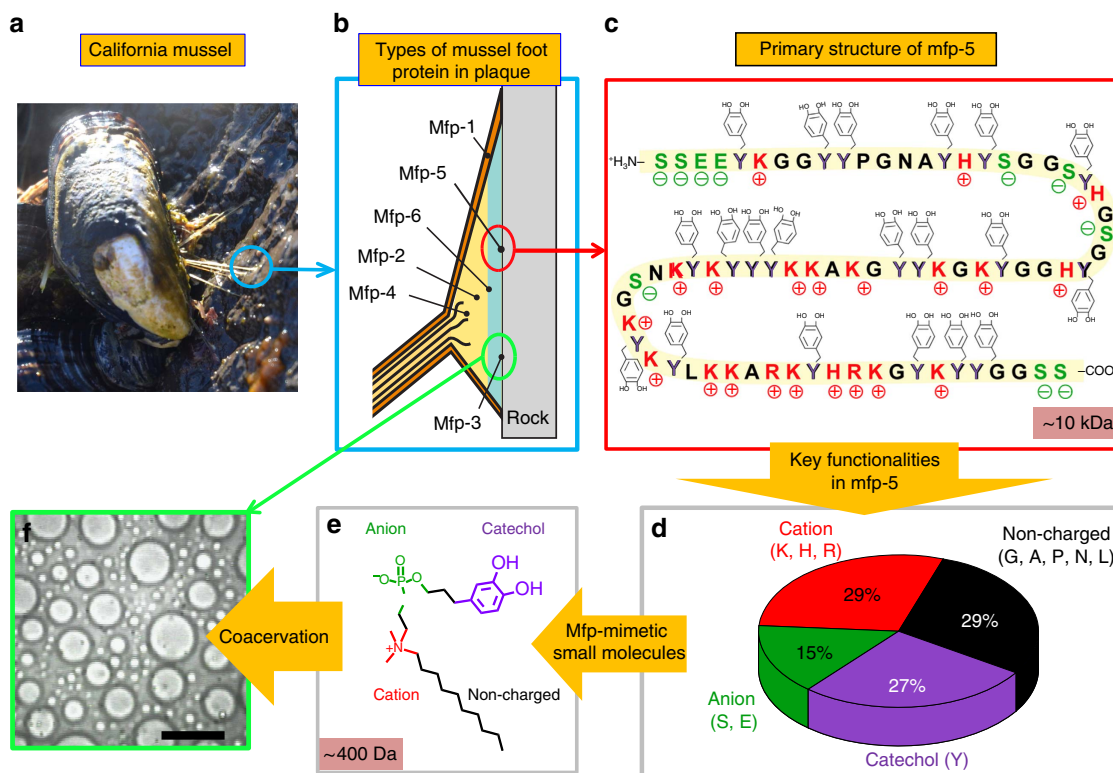


Figure 1 | The key features of natural and translated mussel adhesion. (a) A mussel anchored by byssal threads and plaques to a rock in the intertidal zone (Goleta Pier, California). (b) Schematic of the distribution of different mfps in a plaque. (c) Primary sequence of mfp-5; S (green) denotes phosphoserine. (d) Pie chart of key functionalities in mfp-5. (e) One example (Z-Cat-C10) of a zwitterionic surfactant inspired by mfp-5. (f) Light micrograph image of liquid-phase-separated Z-Cat-C10 at 100 mg ml^{-1} concentration. The scale bar on e corresponds to $200 \mu\text{m}$.

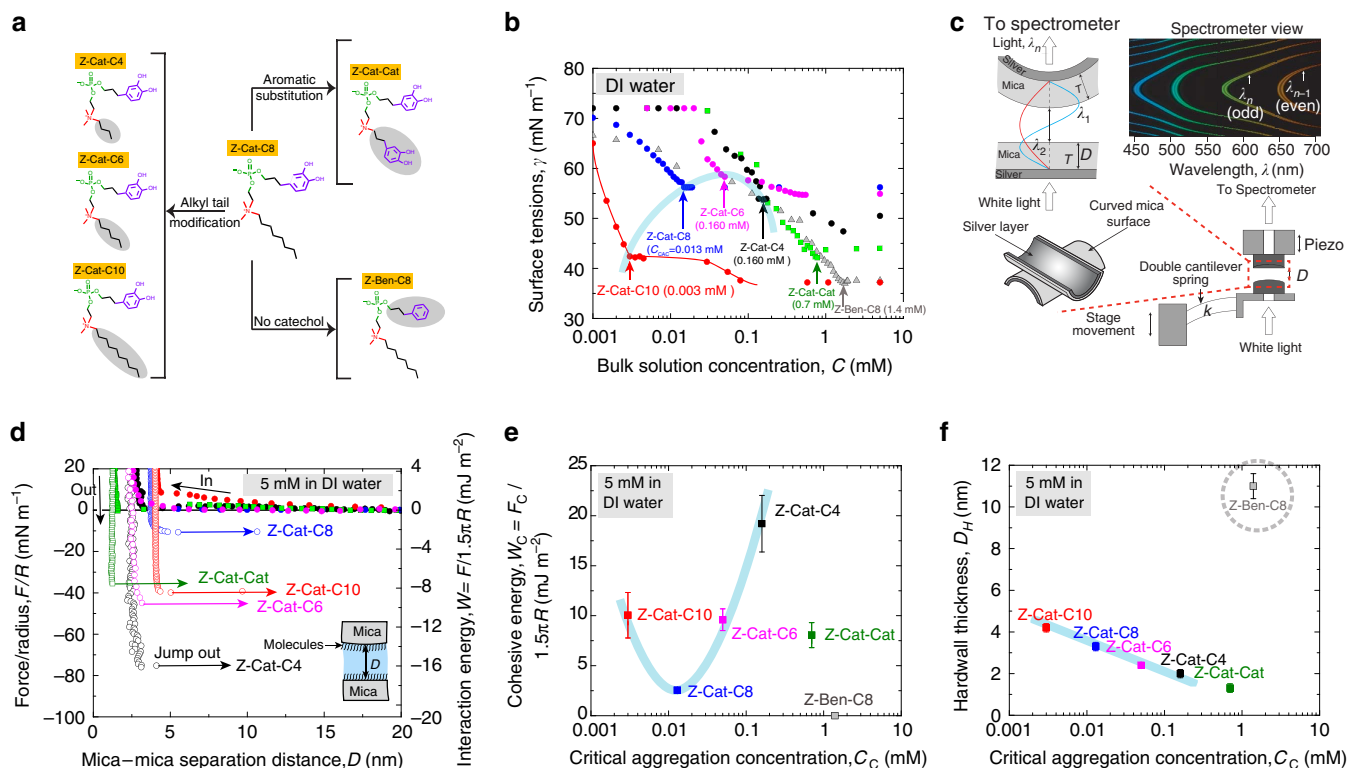


Figure 2 | Aggregation and surface physics behaviour of mfp-mimetic zwitterions. (a) Summary of the engineered homologues. Features varied include alkyl chain length, aromatic substitution, with/without catechol. (b) CAC of each homologue is deduced from the final inflection point in the plot of log concentration versus surface tension as measured by the Wilhelmy plate technique. (c) Schematic of the multiple beam interferometry (MBI) technique used in the SFA, showing the fringes of equal chromatic order used to measure the hard-wall thickness and interfacial energy of interaction between the zwitterionic films (technical details in the Supplementary Methods). (d) Representative force versus distance plots between mica surfaces coated with thin zwitterionic films adsorbed from 5 mM aqueous dispersions of Z-Cat-C10 (red), Z-Cat-C8 (blue), Z-Cat-C6 (pink), Z-Cat-C4 (black) and Z-Cat-Cat (green), respectively. The work of cohesion, W_c (minimum potential well of W versus D , y axis, right), is synonymous with the interaction energy of the zwitterions, and did not change for contact times (t_c) ranging from 2 min to 12 h. Surface forces were measured during approach and separation of the surfaces, respectively. (e) Plot of the homologue interaction energies versus CAC. (f) Plot of the homologue hard-wall thickness versus CAC. Trend dashed lines (light blue) were added as a visual aid in e and f. The error bars indicate s.d.'s ($n=5$, independent experiments). DI, deionized.

(~15 mol%), cationic residues (~29 mol%), Dopa (~27 mol%) and assorted non-charged (~29 mol%) (Fig. 1)²². Accordingly, the chemical complexity of mfps was reduced, and adhesion and coacervation were recapitulated by a strategic combination of functionalities in the zwitterionic platform (Fig. 1e,f). Various homologues were designed by replacing one or both alkyl chains with mfp-mimetic functionalities (Fig. 2a) and their interfacial and adhesive properties were investigated.

Interfacial properties and redox stability. The aggregation tendency of each homologue in water was assessed by the critical aggregation concentration (CAC). The CAC is the concentration at which further addition of solute molecules to a solvent makes them go into finite-sized aggregates while the monomer concentration remains unchanged²⁹. The CAC was determined from the solution surface tension of varying homologue concentrations in deionized water (NB the red line of Z-Cat-C10 in Fig. 2b) by Wilhelmy plate tensiometry. Figure 2b shows that decreasing alkyl tail length increases the CAC gradually from Z-Cat-C10 to -C8, -C6 and -C4 (parabolic dashed line drawn in light blue from Z-Cat-C10 to -C4), consistent with thermodynamic predictions²⁹. Conversely, aromatic substitution (Fig. 2a) increased CAC significantly. The substitution of the catechol of Z-Cat-C8 by a benzene (Fig. 2a) also increased CAC. On the basis of cyclic

voltammetry combined with ultraviolet-visible spectroscopy, the oxidative stability of catechol functionalities in all zwitterionic homologues (for example, $E_{1/2}$ of Z-Cat-C10 ~ +0.25 V at 1 mV s^{-1}) was significantly increased by comparison with 4-methylcatechol (completely solvent accessible, $\Delta E_{1/2} \sim +0.12 \text{ V}$ in deionized water at 1 mV s^{-1}), suggesting a highly stabilizing environment in the dispersion (Supplementary Fig. 1).

Surface force measurements and interfacial interaction study.

Thin films of the zwitterionic homologues were deposited on mica surfaces by adsorption from 5 mM solution (>CAC for all homologues; for concentrations below CAC see Supplementary Discussion), and investigated by the surface forces apparatus (SFA; Fig. 2c), atomic force microscopy (AFM; Supplementary Figs 4, 17 and 18) and quartz crystal microbalance with dissipation (QCM-D; Supplementary Figs 5 and 6). Surface force measurements between symmetric thin films on mica were investigated in the SFA. On approach of the two surfaces, Z-Ben-C8 films showed regular bilayer repulsion and jump-in instabilities typical for surfactant layers (Supplementary Fig. 8), whereas the catecholic homologues showed only slight or no repulsion (Fig. 2d). Z-Cat-C4 ($19.2 \pm 2.4 \text{ mJ m}^{-2}$) exhibited the greatest cohesion (or adhesion) energies in deionized water, followed by Z-Cat-C10 ($10.1 \pm 2.3 \text{ mJ m}^{-2}$), Z-Cat-C6 ($9.6 \pm 1.1 \text{ mJ m}^{-2}$),

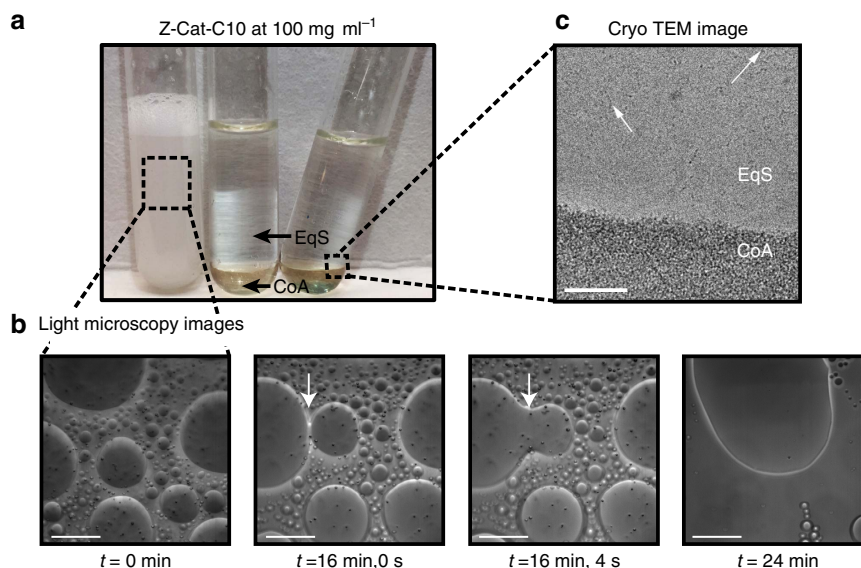


Figure 3 | Fluid-fluid phase separation of mfp-mimetic zwitterions. (a) Phase separation of Z-Cat-C10 (100 mg ml^{-1}) in 4-mm-diameter glass test tubes. Shown are the turbid dispersions of coacervate microdroplets (left) and the bulk-separated phases with the denser coalesced coacervate phase on the bottom (middle) and tilted to emphasize the fluidity of both phases (right). (b) Light micrographs showing the time course of coacervate coalescence in Z-Cat-C10 at 0–24 min. The 16 min, 4 s image shows coalescence of two microdroplets. Scale bar, $100 \mu\text{m}$. (c) Cryo-TEM image of the dense phase; the image of turbid dispersion is similar. White arrows indicate same small aggregations in both equilibrium solution (EqS) and coacervate phase (CoA), an area of a large aggregate of those smaller aggregates seen in the lower part of the field of view. Scale bar, 100 nm .

Z-Cat-Cat ($8.1 \pm 1.3 \text{ mJ m}^{-2}$) and Z-Cat-C8 ($2.5 \pm 0.3 \text{ mJ m}^{-2}$) (Fig. 2e). Notably, the interaction energies of Z-Cat-C10, -C8, -C6 and -C4 were closely correlated with the CAC (light blue parabola drawn in the plot in Fig. 2e as in Fig. 2b).

The hard-wall thickness (the limiting distance between the mica surfaces during the approach run in the SFA) of each homologue was measured and correlated with the CAC (Fig. 2f) corresponding to the catechol-containing zwitterions, which formed strongly cohesive ($W_c = 2.2\text{--}21.6 \text{ mJ m}^{-2}$) bilayers ($0.5\text{--}2.0 \text{ nm}$). In contrast, the non-catecholic Z-Ben-C8 formed multilayered films ($\sim 5 \text{ nm}$) without cohesive tendencies. In the catechol-containing homologues with alkyl tails (Fig. 2a), for example, Z-Cat-C10, -C8, -C6 and -C4, the hard-wall thickness and CAC were both correlated with alkyl tail length (light blue line in Fig. 2f).

Z-Cat-C10, which exhibited the lowest CAC among the homologues and readily phase separated into dense visible coacervates and equilibrium solution at high concentrations (100 mg ml^{-1}), was chosen for further scrutiny (Fig. 3a). Coalescence of the coacervate microdroplets in bulk solution was observed by microscopy (Fig. 3b and Supplementary Movie 1), and spreading of coacervates over a glass substrate was recorded on an inverted microscope (Supplementary Movie 2). Cryogenic transmission electron microscopy (cryo-TEM) images (Fig. 3c and Supplementary Figs 13 and 14) showed small micelle-like aggregates in both equilibrium solution and coacervate phases.

Mussels rely on quinone-mediated protein crosslinking to increase plaque cohesion. o-Quinones are produced by the two-electron oxidation of targeted Dopa residues²². Accordingly, we oxidized the catechol in Z-Cat-C10 with sodium periodate resulting in a stoichiometric -2H^+ and $-2e^-$ oxidation to o-quinone¹⁹. Given the nanoNewton precision of the SFA, we measured the adhesion of monomolecular layers of Z-Cat-C10 on mica. SFA force–distance profiles between surfaces allow the measurement of adhesion forces that can be translated into

adhesion energies (W_{ad}) by the Johnson–Kendall–Roberts theory for soft deformable surfaces^{29,30}. Analysis by SFA showed that the observed cohesion or adhesion energy correlated well with the symmetric or asymmetric oxidation of catechol by periodate⁷. After symmetric periodate oxidation (Fig. 4a), cohesion initially decreased by 50% for contact times of $\leq t_c = 10 \text{ min}$, but then rebounded after $t_c = 60\text{-min}$ contact times. Conversely, asymmetric oxidation, that is, all catechol on one side and all quinone on the other (Fig. 4b), maintained the initial adhesion for contact times of $\leq t_c = 10 \text{ min}$, followed by a 50% increase in adhesion after a $t_c = 60\text{-min}$ contact time. The loss^{22,24} and subsequent recovery²² of adhesion, respectively, following oxidation were previously explained as the loss of H-bonding interactions because quinones are exclusively H-bond acceptors (short term), followed by the quinone-mediated formation of covalent crosslinks (long term). The high adhesion ($W_{\text{ad}} \sim 50 \text{ mJ m}^{-2}$) obtained after $t_c = 12 \text{ h}$ of compressive contact, contrasts with $\leq t_c = 10 \text{ min}$ and $t_c = 1 \text{ h}$ contacts. According to the post-oxidation analyses, covalent crosslinks formed within and between the thin films ($\sim 2\text{--}4 \text{ nm}$) (Fig. 4c).

Not limited to mica (Fig. 4d), 5 mM Z-Cat-C10 formed thin, molecularly smooth ($\sim 2 \text{ nm}$) films on silicon wafers (Supplementary Fig. 15) and copper (Supplementary Fig. 16). The wet and dry adhesion of these films (Supplementary Figs 17–20) on silicon wafers (SiO_2 , root mean squared (r.m.s.) surface roughness $< 1 \text{ nm}$) and copper ($\text{CuO}_2/\text{Cu}(\text{OH})_2$, r.m.s. surface roughness $\sim 2 \text{ nm}$) surfaces was measured using silica (SiO_2) probes in the AFM (Fig. 4e). The surfaces were prepared by spreading 5 mM Z-Cat-C10 over the surfaces, followed by thorough rinsing and adhesive testing (Fig. 4f). The wet work of adhesion ($W_{\text{ad}} = F_{\text{ad}}/1.5\pi R$), $\sim 7.7 \text{ mJ m}^{-2}$ for the SiO_2 and SiO_2 interface, resembled $W_{\text{ad}} \sim 7.0 \text{ mJ m}^{-2}$ reported for catechol-functionalized polysiloxanes and SiO_2 interface³¹, and $\sim 0.1 \text{ mJ m}^{-2}$ for adhesion between the $\text{CuO}_2/\text{Cu}(\text{OH})_2$ and SiO_2 surfaces. After air drying the surfaces for $\sim 5 \text{ min}$, the adhesion (W_{ad}) between $\text{CuO}_2/\text{Cu}(\text{OH})_2$ and SiO_2 surfaces

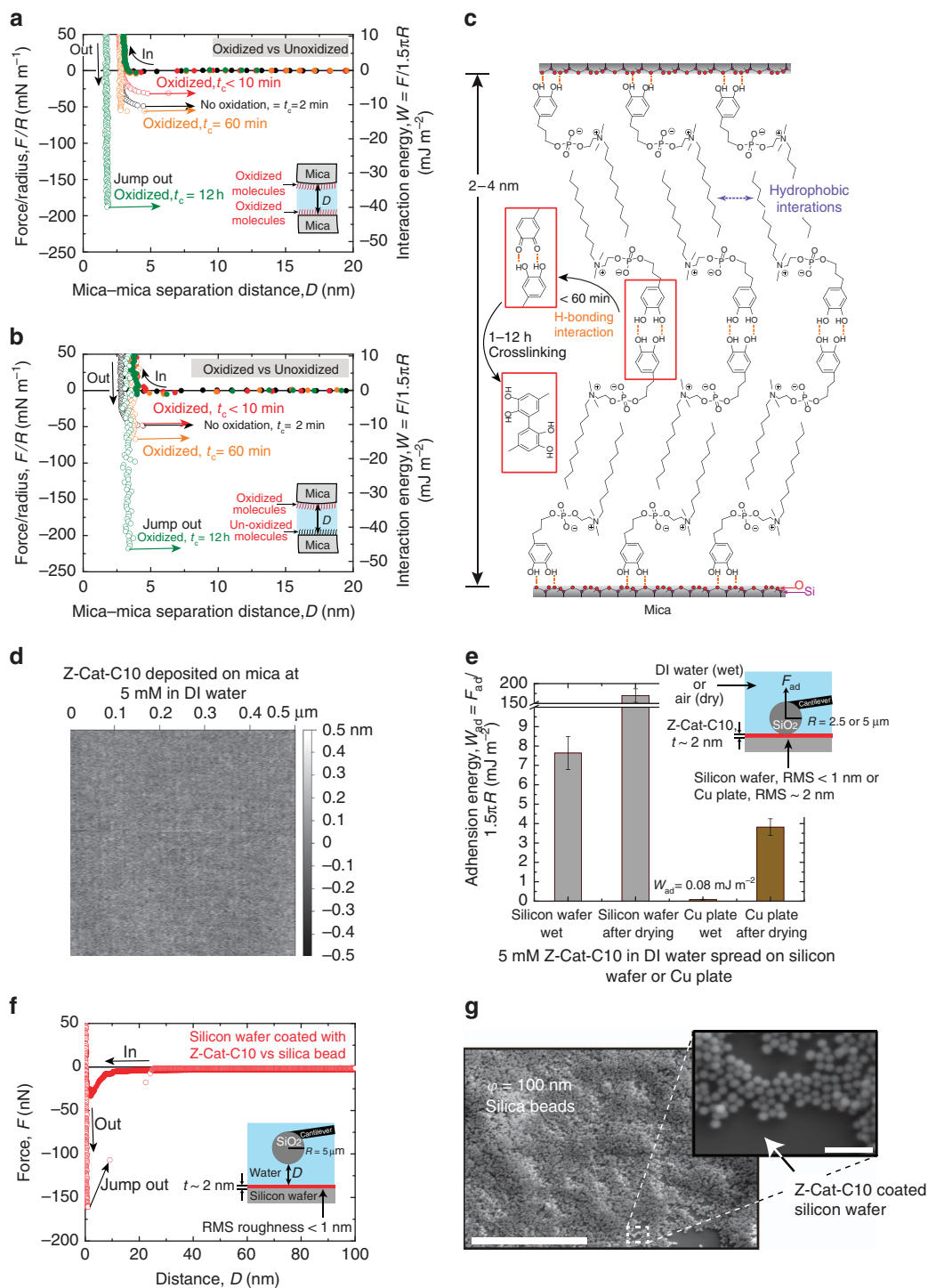


Figure 4 | Atomically smooth and thin nano-adhesives from mfp-mimetic zwitterion. (a,b) Representative force versus (vs) distance plots of symmetric (a) and asymmetric (b) periodate oxidized Z-Cat-C10 films on mica. Before periodate, the work of adhesion W_{ad} did not change for contact times (t_c) from 2 min to 12 h (black). After oxidation with periodate (250 μM), $t_c \leq 10$ min (red points), $t_c = 60$ min (orange) and $t_c = 12$ h (green). Filled and open circles represent the forces measured during approach and separation of the surfaces, respectively. (c) Cartoon of the two self-assembled nano-glue layers (upper and lower, respectively) and the interface. (d) AFM image of atomically smooth adhesive layer formed from 5 mM Z-Cat-C10 on mica (the layer on SiO_2 and $\text{CuO}_2/\text{Cu}(\text{OH})_2$ shown in Supplementary Figs 15 and 16, respectively). (e) Adhesion energy ($W_{ad} = F_{ad}/1.5\pi R$) of the nano-glue from Z-Cat-C10 measured on silicon wafer and copper plate, where adhesion force F_{ad} (minimum of the potential well of the F versus D curves obtained from AFM measurements) and R (radius of silicon dioxide probe). (f) Representative force versus distance plots of the nano-glue from 5 mM Z-Cat-C10 in AFM. (g) SEM image of underwater glued nano silica beads ($\phi = 100$ nm) on silicon wafer by the nano-glue from 5 mM Z-Cat-C10. The error bars indicate s.d.'s ($n = 5$, independent experiments). Scale bar, 500 μm ; inset scale bar, 500 nm. DI, deionized.

increased significantly to $\sim 4 \text{ mJ m}^{-2}$ and to $\sim 175 \text{ mJ m}^{-2}$ between SiO_2 and SiO_2 surfaces, which, in the latter case, is 50-fold greater than the W_{ad} ($\sim 3.5 \text{ mJ m}^{-2}$) for catecholic polysiloxane adhesion to SiO_2 as calculated from the F_{ad} (83 nN) measured using silica probes ($\phi = 5 \mu\text{m}$) in AFM³¹. Comparatively weaker adhesion to the copper plate is tentatively attributed to higher r.m.s. and hydroxides on its surface measured by AFM and X-ray photoelectron spectroscopy (XPS), respectively (Supplementary Figs 21–26). We also prepared a suspension of silica beads ($\phi = 100 \text{ nm}$) in deionized water, and spread it over a silicon wafer previously coated with 5 mM Z-Cat-C10. The silica beads remained glued to the film, even after rinsing with pulsed jets of running tap water (0.24 MPa; Fig. 4g).

Discussion

Catechol-functionalized zwitterionic surfactants are clearly more than detergents, and show the following favourable attributes as adhesive primers: (1) they aggregate in water as dense fluidic coacervates at concentrations above the CAC; (2) the coacervates spread uniformly over surfaces; (3) in confinement in the SFA, the coacervates rearrange as paired bilayers ($\sim 2.5\text{-nm}$ thickness) with the catecholic head groups facing the mica surface on one side and bulk solvent on the other; (4) the coacervate environment stabilizes catechols by $\sim +0.1 \text{ V}$ against oxidation; and (5) following periodate treatment, adhesion of thin films of Z-Cat-C10 on mica approaches $W_{\text{ad}} \sim 50 \text{ mJ m}^{-2}$ —a new high value for catechol-mediated adhesion.

The results reveal Z-Cat-C10 adhesion on mica to be two- to three-fold greater than mfp-5 (14 mJ m^{-2}) (ref. 22) and the new mfp-amyloid recombinant fusion protein (21 mJ m^{-2}) (ref. 24). Results obtained before and after periodate oxidation of Z-Cat-C10 suggest the following failure modes: before periodate, the work of adhesion averaged $\sim 20 \text{ mJ m}^{-2}$. Because the hydrophobic bilayer and catechol-to-mica contacts are strong, the weaker inter-catechol H-bonding between the two bilayers (Fig. 4c) unzips during separation. After covalent aryl-aryl coupling with periodate, the adhesion failed at $\sim 50 \text{ mJ m}^{-2}$, which is commensurate with the energy required to separate the two halves of a lipid bilayer leaflet³², thus suggesting that adhesion to the mica surface is stronger than $\sim 50 \text{ mJ m}^{-2}$.

Because the SFA-based work of adhesion (units J m^{-2}) is difficult to relate to reported bulk adhesion properties (J m^{-3}), we shall compare it with peel fracture energy. With native mussel plaques deposited onto silica, peel fracture energy¹ was 100 J m^{-2} , which resembles the energy of high-performance adhesive polystyrene; polyvinylpyrrolidone (PS/PVP) blends on silicon²⁸. The magnitude of disparity between the work of adhesion and peel fracture energy is striking but plausible. In tests of symmetrically deposited Z-Cat-C10, the paired bilayer structure (Fig. 4c) offers little opportunity for energy dissipation via sacrificial bonds and hidden lengths³³, whereas in the plaque, molecular scaffolds of different length scales exist³⁴. The relationships between the adhesive surface primers and their overlying molecular scaffolds are not well understood. Although the catechol-functionalized zwitterionic surfactants were designed to be adhesive primers, some bulk tests in lap shear or a three-point bending peel mode on stainless steel (SS304) (Supplementary Fig. 12) showed unexpected gap-filling capabilities and strengths of $\sim 1 \text{ MPa}$ or $\sim 20 \text{ N cm}^{-1}$, suggesting that stacked bilayers as shown in Fig. 4c may not be limited to two layers.

In summary, we show that a synthetic low-molecular-weight catecholic zwitterionic surfactant mimics the strong adhesive priming and self-coacervating properties of mfps. The high wet-cohesion (or -adhesion) energies ranged from ~ 20 to $\sim 50 \text{ mJ m}^{-2}$ for uncrosslinked and crosslinked films,

respectively. This study underscores the importance of catechols and of maintaining a balance⁴ between hydrophobic and electrostatic interactions for tuning or optimizing both coacervation and adhesion. These catecholic zwitterions are adaptable as coatings or adhesive primers^{14,28} for diverse surfaces and, given their uniformly thin ($< 4 \text{ nm}$) and strong glue layers, hold particular promise as a new tool for nanofabrication^{25–27,35} (please see Supplementary Note and Discussion for appropriate details).

Methods

Synthesis. The zwitterionic surfactants were synthesized based on a previously described procedure²³ (Supplementary Methods).

Critical aggregation concentration. Aqueous colloidal dispersions of each homologue were prepared in deoxygenated deionized water. The CAC was determined from the solution surface tension of varying homologue concentrations in deionized water (for example, see the red line of Z-Cat-C10 in Fig. 2b) by Wilhelmy plate tensiometry and has been described elsewhere³⁶. Use of the CAC instead of Critical Micelle Concentration (CMC) here is a hedge to accommodate our uncertainty about whether micelles or other soluble aggregates were forming.

Cyclic voltammetry. Cyclic voltammetry (CV) was performed on a Versastat 3 potentiostat from Ametek Co. (Berwyn, PA). These analyses were carried out using a three-electrode cell: a Pt wire as the counter electrode; an Ag/AgCl reference electrode; and a carbon paste electrode (CPE) served as the working electrode. Carbon paste electrode is the best choice for adhesive materials because of its ability to be completely polished before each experiment.

Measuring adhesion and cohesion energies. The adhesion/cohesion energy of the synthetic zwitterionic molecules was investigated in SFA (SurForce LLC, Santa Barbara, CA). Two molecularly smooth freshly cleaved back-silvered mica surfaces glued on cylindrical silica discs of radius of curvature, $R \sim 2 \text{ cm}$ were mounted in the SFA and $50 \mu\text{l}$ of a colloidal dispersion of the synthetic molecules in deionized water was injected between the surfaces at different concentrations ($C = 0.5\text{--}5 \text{ mM}$) and the forces between the thin films of the molecules were measured by multiple beam interferometry³⁷. The adhesion forces between Z-Cat-C10 molecules on various surfaces, for example, silica and copper, were also measured by AFM (MFP-3D, Asylum Research, Goleta, CA) in deionized water and ambient conditions, respectively, at room temperature. AFM probes with a silicon dioxide particle (10, 5 and $1 \mu\text{m}$, respectively) on a silicon nitride (SN) cantilever (-0.6 N m^{-1}) were purchased from Novascan Technologies, Inc. (Ames, IA). Cantilever spring constants were measured for each force run. Images of Z-Cat-C10 coating on silicon wafer and copper plates were visualized in an AFM.

Cryo-TEM. Cryo-TEM vitrified specimens were prepared in a controlled environment vitrification system at 25°C and 100% relative humidity. The procedure is described in detail elsewhere³⁸. About $3 \mu\text{l}$ of the sample was applied onto a perforated (lacey) carbon film-coated 200 mesh copper TEM grid. Excess liquid was blotted with filter paper, and the specimen was immediately plunged into liquid ethane at its freezing point (-183°C). The vitrified specimens were 240 transferred to a 626 Gatan cryo-holder, using it transfer station, and imaged at 120 kV acceleration voltage in an FEI Tecnai T12 G² TEM, using low-dose imaging to minimize electron-beam radiation damage. Typical electron exposures were 10 to $15 \text{ e}^- \text{ \AA}^{-2}$. The specimens were kept in the TEM at about -175°C . Images were digitally recorded with a Gatan US1000 high-resolution ($2\text{it} \times 2\text{high}$ -resolution 2charge-coupled device camera, using the Digital Micrograph software).

QCM-D. A 'static cell' (often called 'Open Model') QCM-D (Q-Sense, Biolin Scientific, Linthicum Heights, MD) was employed to qualitatively show the adsorption of the zwitterionic molecules onto mineral and metal oxide surfaces (Supplementary Methods).

XPS. XPS (Kratos Axis Ultra, Kratos Analytical, Manchester UK) was conducted with survey scans at a pass energy of 160 eV , and high-resolution scans at a pass energy of 40 eV . Nano-layer adhesion to silica surface was imaged with SEM after rinsing silica bead (diameter $\phi = 100 \text{ nm}$) dispersion (10 mg ml^{-1} in deionized water), spread on a silicon wafer coated with Z-Cat-C10, thoroughly with deionized water.

References

- Desmond, K., Zaccchia, N. A., Waite, H. J. & Valentine, M. Dynamics of mussel plaque detachment. *Soft Matter* **11**, 6832–6839 (2015).
- Lee, B. P., Messersmith, P. B., Israelachvili, J. N. & Waite, J. H. Mussel-inspired adhesives and coatings. *Annu. Rev. Mater. Res.* **41**, 99–132 (2011).

3. Faure, E. *et al.* Catechols as versatile platforms in polymer chemistry. *Prog. Polym. Sci.* **38**, 236–270 (2013).
4. Seo, S. *et al.* Micro-phase behavior and enhanced wet-cohesion of synthetic copolyampholytes inspired by a mussel foot protein. *J. Am. Chem. Soc.* **137**, 9214–9217 (2015).
5. Lee, H., Scherer, N. & Messersmith, P. Single-molecule mechanics of mussel adhesion. *Proc. Natl Acad. Sci. USA* **103**, 12999–13003 (2006).
6. Shafiq, Z. *et al.* Bioinspired underwater bonding and debonding on demand. *Angew. Chem. Int. Ed.* **51**, 4332–4335 (2012).
7. Ahn, B. K., Lee, D. W., Israelachvili, J. N. & Waite, J. H. Surface-initiated self-healing of polymers in aqueous media. *Nat. Mater.* **13**, 867–872 (2014).
8. Krogsgaard, M., Behrens, M. A., Pedersen, J. S. & Birkedal, H. Self-healing mussel-inspired multi-pH-responsive hydrogels. *Biomacromolecules* **14**, 297–301 (2013).
9. Wei, W. *et al.* A mussel-derived one component adhesive coacervate. *Acta Biomater.* **10**, 1663–1670 (2014).
10. Rodriguez, N. R. M. *et al.* Mussel adhesive protein provides cohesive matrix for collagen type-1 α . *Biomaterials* **51**, 51–57 (2015).
11. Wang, J. *et al.* Influence of Binding-Site Density in Wet Bioadhesion. *Adv. Mater.* **20**, 3872–3876 (2008).
12. Hwang, D. S. *et al.* Viscosity and interfacial properties in a mussel-inspired adhesive coacervate. *Soft Matter* **6**, 3232–3236 (2010).
13. Stewart, R. J., Wang, C. S. & Shao, H. Complex coacervates as a foundation for synthetic underwater adhesives. *Adv. Colloid Interface Sci.* **167**, 85–93 (2011).
14. Skeist, I. *Handbook of Adhesives* (Van Nostrand Reinhold Co, 1977).
15. Wei, W., Yu, J., Broomell, C., Israelachvili, J. N. & Waite, J. H. Hydrophobic enhancement of dopa-mediated adhesion in a mussel foot protein. *J. Am. Chem. Soc.* **135**, 377–383 (2013).
16. Yamamoto, H. Synthesis and adhesive studies of marine polypeptides. *J. Chem. Soc. Perkin Trans. 1*, 613–618 (1987).
17. Deming, T. Mussel byssus and biomolecular materials. *Curr. Opin. Chem. Biol.* **3**, 100–105 (1999).
18. Winslow, B. D., Shao, H., Stewart, R. J. & Tresco, P. A. Biocompatibility of adhesive complex coacervates modeled after the sandcastle glue of *Phragmatopoma californica* for craniofacial reconstruction. *Biomaterials* **31**, 9373–9381 (2010).
19. Liu, B., Burdine, L. & Kodadek, T. Chemistry of periodate-mediated cross-linking of 3,4-dihydroxyphenylalanine-containing molecules to proteins. *J. Am. Chem. Soc.* **128**, 15228–15235 (2006).
20. Yu, M. & Deming, T. J. Synthetic polypeptide mimics of marine adhesives. *Macromolecules* **31**, 4739–4745 (1998).
21. Martinez Rodriguez, N. R., Das, S., Kaufman, Y., Israelachvili, J. N. & Waite, J. H. Interfacial pH during mussel adhesive plaque formation. *Biofouling* **31**, 221–227 (2015).
22. Danner, E. W., Kan, Y. J., Hammer, M. U., Israelachvili, J. N. & Waite, J. H. Adhesion of mussel foot protein mfp-5 to mica: an underwater superglue. *Biochemistry* **51**, 6511–6518 (2012).
23. Peresyppkin, A. V. & Menger, F. M. Zwitterionic geminis. Coacervate formation from a single organic compound. *Org. Lett.* **1**, 1347–1350 (1999).
24. Zhong, C. *et al.* Strong underwater adhesives made by self-assembling multi-protein nanofibres. *Nat. Nanotechnol.* **9**, 858–866 (2014).
25. Gandhi, D. D. *et al.* Annealing-induced interfacial toughening using a molecular nanolayer. *Nature* **447**, 299–302 (2007).
26. Magasinski, A. *et al.* High-performance lithium-ion anodes using a hierarchical bottom-up approach. *Nat. Mater.* **9**, 353–358 (2010).
27. Hirakata, H., Kitamura, T. & Yamamoto, Y. Direct measurement of interface strength between copper submicron-dot and silicon dioxide substrate. *JSME Int. J. Ser. A* **47**, 324–330 (2004).
28. Jeong, J. W. *et al.* High-resolution nanotransfer printing applicable to diverse surfaces via interface-targeted adhesion switching. *Nat. Commun.* **5**, 5387 (2014).
29. Israelachvili, J. N. *Intermolecular and Surface Forces: Revised 3rd edn* (Academic, 2011).
30. Das, S. *et al.* JKR theory for the stick-slip peeling and adhesion hysteresis of gecko mimetic patterned surfaces with a smooth glass surface. *Langmuir* **29**, 15006–15012 (2013).
31. Heo, J. *et al.* Improved performance of protected catecholic polysiloxanes for bioinspired wet adhesion to surface oxides. *J. Am. Chem. Soc.* **134**, 20139–20145 (2012).
32. Meyer, E. E., Rosenberg, K. J. & Israelachvili, J. Recent progress in understanding hydrophobic interactions. *Proc. Natl Acad. Sci. USA* **103**, 15739–15746 (2006).
33. Fantner, G. E. *et al.* Sacrificial bonds and hidden length dissipate energy as mineralized fibrils separate during bone fracture. *Nat. Mater.* **4**, 612–616 (2005).
34. Tamarin, A., Lewis, P. & Askey, J. The structure and formation of the byssus attachment plaque in *Mytilus*. *J. Morphol.* **149**, 199–221 (1976).
35. Betancourt, T. & Brannon-Peppas, L. Micro- and nanofabrication methods in nanotechnological medical and pharmaceutical devices. *Int. J. Nanomed.* **1**, 483–495 (2006).
36. Das, S., Donaldson, Jr S. H., Kaufman, Y. & Israelachvili, J. N. Interaction of adsorbed polymers with supported cationic bilayers. *RSC Adv.* **3**, 20405–20411 (2013).
37. Israelachvili, J. Thin-film studies using multiple-beam interferometry. *J. Colloid Interf. Sci.* **44**, 259–272 (1973).
38. Talmon, Y. Transmission electron microscopy of complex fluids: the state of the art. *Ber. Bunsenges. Phys. Chem* **100**, 364–372 (1996).

Acknowledgements

We acknowledge financial support from the Office of Naval Research N000141310867, National Institute of Health R01 DE018468 and National Science Foundation MRSEC DMR-1121053. The cryo-TEM work was performed at the Technion Laboratory for Electron Microscopy of Soft Matter, supported by the Technion Russell Berrie Nanotechnology Institute (RBNI). We thank Sachin Handa for helpful discussions regarding the molecular syntheses and Mary Raven in NRI/MCDB Microscopy Facility.

Author contributions

B.K.A. coordinated the research team and collated the overall research; S.D. performed and interpreted surface characterizations including those from on the SFA; R.L. synthesized mfp-mimetic molecules; Y.K. performed and interpreted AFM and SEM; N.R.M. performed the SFA and QCM-D; R.M. performed and interpreted Cyclic Voltammetry and ultraviolet–visible spectroscopy; E.K. and Y.T. performed and interpreted cryo-TEM; B.H.L. designed the molecular syntheses; J.N.I. and J.H.W. supervised the overall research; B.K.A. and J.H.W. wrote the manuscript; B.K.A. and S.D. made the figures; all authors contributed to revising the manuscript and writing the supplementary section.

Additional information

Supplementary Information accompanies this paper at <http://www.nature.com/naturecommunications>

Competing financial interests: The authors declare no competing financial interests.

Reprints and permission information is available online at <http://npg.nature.com/reprintsandpermissions/>

How to cite this article: Ahn, B. K. *et al.* High-performance mussel-inspired adhesives of reduced complexity. *Nat. Commun.* 6:8663 doi: 10.1038/ncomms9663 (2015).



This work is licensed under a Creative Commons Attribution 4.0 International License. The images or other third party material in this article are included in the article's Creative Commons license, unless indicated otherwise in the credit line; if the material is not included under the Creative Commons license, users will need to obtain permission from the license holder to reproduce the material. To view a copy of this license, visit <http://creativecommons.org/licenses/by/4.0/>